Research On The Fractal and Percolation Characteristics of Coal-Based Porous Media For Filtration and Impregnation

Qili Wang (scetwql@cumt.edu.cn)
China University of Mining and Technology
Jiarui Sun
China University of Mining and Technology
Yuehu Chen
China University of Mining and Technology
Yuyan Qian
China University of Mining and Technology
Shengcheng Fei
China University of Mining and Technology
Sheng Yan
China University of Mining and Technology

Research Article

Keywords: Coal-based porous media, Mercury intrusion porosimetry (MIP), Fractal characteristics, Percolation

Posted Date: October 1st, 2021

DOI: https://doi.org/10.21203/rs.3.rs-948994/v1

Research on the Fractal and Percolation Characteristics of Coal-based Porous Media for filtration and impregnation

* Wang Qili, Sun Jiarui, Chen Yuehu, Qian Yuyan, Fei Shengcheng, Yan Sheng

1. Key Laboratory of Coal Processing and Efficient Utilization, Ministry of Education, China University of Mining and Technology, Xuzhou, 221116, P.R. China

* Corresponding authors: E-mail: scetwql@cumt.edu.cn.

Abstract: In order to distinguish the difference in the heterogeneous fractal structure of porous graphite used for filtration and impregnation, the fractal dimensions obtained through the mercury intrusion porosimetry (MIP) along with the fractal theory were used to calculate the volumetric FD of the graphite samples. The FD expression of the tortuosity along with all parameters from MIP test was optimized to simplify the calculation. In addition, the percolation evolution process of mercury in the porous media was analyzed in combination with the experimental data. As indicated in the analysis, the FDs in the backbone formation regions of sample vary from 2.695 to 2.984, with 2.923 to 2.991 in the percolation regions and 1.224 to 1.544 in the tortuosity. According to the MIP test, the mercury distribution in porous graphite manifested a transitional process from local aggregation, gradual expansion, and infinite cluster connection to global connection.

Keywords: Coal-based porous media, Mercury intrusion porosimetry (MIP), Fractal characteristics, Percolation

1 Introduction

Over years, the study of fractal porous media has caught intensive attentions of many scholars and researchers. The structural characterization and description have been considered as the foundation for the study of thermophysical phenomena, such as the flow, phase transition, heat and mass transfer in porous media [1-3]. Due to the randomness and heterogeneity of the structures in porous media, the traditional Euclidean geometry fails to describe the structural characterization accurately. However, the fractal geometry has gradually adopted by many researchers and proven to be valid and fruitful. The fractal theory has been considered as a powerful tool in studying fractal geometry and fractal phenomena in nature [4]. Some researchers, including Katz, Winslow, Krohn and Tyler, et al., have successfully described the structural characteristics of porous media such as sandstone, rock, coal char, cement and soil based on the fractal method, derived the expressions of fractal dimension (FD), proposed the physical meaning and obtained the parameters [5-10].

Measurement and description are two key steps in the structural characterization of fractal media. Image processing methods are often used to characterize the fractal features of 2- dimensional (2-D) planes of a porous media. For example, a 2-D image of a porous media can be obtained through the scanning electron microscopy (SEM). The FD of the 2-D fractal structure can be developed by box-counting method, the area-circumference method or the area-radius method [11-13].

Regarding the 3-dimensional (3-D) fractal media, the experimental measurement and the image processing method are combined to obtain the structural parameters. Some structural parameters are obtained through experiments with the adoption of mercury intrusion porosimetry (MIP) and nitrogen (N2) low pressure gas adsorption (LPGA). Some parameters are obtained through the image

processing method, such as the micro-CT and SEM. The volumetric of the 3-D porous media can be obtained through the fractal method with the characteristic parameters. Relevant productive researches have been conducted by scholars such as Go´mez-Carracedo et al., Yao et al., and Wu et al. [14-16]. The physical and chemical stability of the porous graphite has contributed to the wide adoption in various fields such as materials, chemicals, biology and environment [17]. In industrial applications such as impregnation and filtration, the effective description of the heterogeneous structure plays a crucial role to study the fluid flow phenomena in porous graphite [18]. Many studies have indicated that the structure of porous graphite demonstrates some typical fractal characteristics, which can be described through the fractal method [19, 20]. In this study, the fractal characteristics of the porous graphite, which was prepared from coal-based raw materials, were described with an optimized method developed to describe the tortuosity fractal dimension. In order to minimize the errors caused by the measurement method and instrument accuracy, only the parameters through the MIP were used to obtain the FDs of volume. Moreover, the evolution process and percolation characteristics of the mercury occupation in porous graphite were analyzed based on the data obtained from the MIP.

2 Experimental

As an effective method for determining the distribution of some mesopores and macropores in porous medium, the MIP is developed based on the Young-Laplace law and Washburn equation to measure complex pore structures [21,22]. Many studies were conducted to measure the pore structure and permeability of porous media through the MIP [23-26].

Porous graphite samples were prepared using coal coke particles as raw materials and medium-temperature coal tar pitch as binder by following different aggregate formulas. Four samples were selected for filtration (No.1-4#) and four for impregnation (No.5-8#). The MIP test was conducted by Micromeritics AutoPore IV 9520, with a maximum pressure of 60,000 psia, a pressure accuracy of 0.01 psia, a pore size measurement range of 3 nm to 1000 μm, and a volumetric accuracy of 0.1 μL. The main steps of the MIP test are provided as follows:

a. The samples were firstly processed into a cylinder shape with a diameter of 8 mm and a height of 10 mm. Sample cylinders were cleaned and dried in the oven for 10 hours at 100℃.
b. The sample was weighed and placed in the sample tube. Tube was sealed with think resins.
c. Measurement in the low-pressure station: Low-pressure tests were performed under the vacuum of less than 50 μmHg. Mercury was removed and the samples were scaled.
d. Measurement in the high-pressure station: Sample was pressurized in the station where the pressure was increased to 30,000 psia.
e. Data collection and process were conducted through the software connected to the test system.

3 Results and discussion

3.1 The Pore structural parameters of porous graphite

Table 1 Main parameters of porous graphite samples from MIP test

Sample No.	1#	2#	3#	4#	5#	6#	7#	8#
Intrusion volume (mL/g)	0.293	0.350	0.242	0.272	0.064	0.054	0.097	0.060
Threshold pressure (psia)	8.49	4.67	13.05	11.19	171.26	127.53	88.03	126.31
Pore diameter (min,nm)	6.03	6.63	7.11	6.61	7.23	7.24	7.14	7.13
Pore diameter (max,um)	323.33	89.30	151.87	146.76	89.15	89.37	217.17	211.9
Average pore diameter (nm)	281.7	227.1	318.6	399.8	74.6	100.8	85.5	66.2
Characteristic length (nm)	21301.5	62998.6	15137.3	15084.3	5056.1	11418.2	8488.2	7440.1
Pore area (m2 /g)	5.354	6.157	3.041	2.726	3.429	2.159	4.523	6.607
Bulk density (g/cm3)	1.305	1.209	1.225	1.189	1.687	1.753	1.624	1.786
Skeletal density (g/cm3)	2.112	2.094	1.743	1.761	1.891	1.937	1.922	1.998
Porosity (%)	38.20	42.25	29.69	32.42	10.79	9.53	15.75	10.67

As shown in Table 1, the samples for filtration (No.1-4#) have the bulk density of 1.189-1.305 g/cm^3, the skeletal density of 1.743-2.112 g/cm^3, the porosity of 29.69- 42.25%, the intrusion volume of 0.242-0.350 mL/g, the threshold pressure of 4.67-13.05 psia, and the average pore diameter of 227.1-399.8 nm. Meanwhile, the samples for impregnation (No.5-8#) have the bulk density of 1.624-1.786 g/cm^3, the skeletal density of 1.891-1.998 g/cm^3, the porosity of 9.53-15.75%, the intrusion volume of 0.054-0.097 mL/g, the threshold pressure of 88.03-171.26 psia, and the average pore diameter of 66.2-100.8 nm. The comparison of filtration samples and impregnation samples suggests that the mercury intrusion volume for the filtration porous graphite is much higher along with a bigger average pore diameter and porosity.

3.2 Fractal characteristics of structure in porous media

3.2.1 Volumetric FD of porous media

For a fractal media with self-similarity is equally divided n times, the relationship among the remaining area, the scale, and the FD can be expressed by Eq. (1) [4, 5].

$$A = \delta^{2-D} \quad (1)$$

Where A is the remaining area, δ is the smallest scale after n divisions and D standards for FD of the 2-D area ($1 < D \le 2$). Eq. (1) shows the relationship among the2-D area (A), the measurement scale (δ) and area FD (D). Similarly, by extending Eq. (1) from a 2-D plane to a 3-D volume, the expression can be obtained as Eq. (2).

$$V \propto \delta^{(3-D_v)} \quad (2)$$

Where V is the volume of the 3-D fractal media and D_v standards for the volumetric of the fractal media.

The box-counting method was widely used to calculate the FD of 2-D fractal images effectively by many researchers. [27,28]. However, applying the box-counting method to obtain the volumetric of the 3-D fractal media is challenging. To calculate volumetric FD of the 3-D fractal media through the box-counting method, various units of 3- D under different scales are needed to conduct multiple box-counting and calculation, which can be difficult and time-consuming [28].

Angulo et al. established an effective method to calculate the FD of a 3-D fractal media [29]. According to the Yong-Laplace theory, when fluid flows through a pore, the capillary pressure depends on the pore size which makes the replacement of geometric scale with the pressure scale possible to measure the intrusion volume and the corresponding pore size under a certain capillary pressure, which has been proven to be effective When the capillary pressure (P_c) is above the threshold pressure (P_t), the intrusion volume tends to rise rapidly. The intrusion volume is related to the pressure and the FD of the media. The relationship among FD, pressure and intrusion volume is shown as follows [29].

$$V = (P_c - P_t)^{(3-D_v)} \quad (3)$$

Taking the logarithm of both sides of Eq. (6) and setting $\Delta P = P_c - P_t$, the following expression can be obtained as Eq. (4).

$$\log(V) = (3 - D_v)\log(P_c - P_t) = (3 - D_v)\log(\Delta P) \quad (4)$$

By simplifying Eq. (4), a FD expression as shown in Eq. (5) is developed.

$$D_v = 3 - \frac{\log(V)}{\log(\Delta P)} \quad (5)$$

Where D_v is the volumetric of fractal media, P_c stands for the capillary pressure, P_t refers to the threshold pressure, V indicates the intrusion volume, respectively. Eq.8 shows a close linear relationship between $\log(V)/\log(\Delta P)$ and FD. Moreover, $3 - D_v$ is the slope of $\log(V)$ and $\log(\Delta P)$.

By measuring the different parameters of $\log(V)$ and $\log(\Delta P)$ experimentally, the volumetric of the fractal medium can be calculated. In MIP test, the boundary between the backbone formation region and the percolation region should be closely monitored, which shows different characteristics. Therefore, the FDs of different regions can be obtained by analyzing the data corresponding to different regions. The double logarithmic curves of V-ΔP for eight porous graphite samples are developed and shown in Fig.1, and the results of FDs and relationship equations are shown in Table 2.

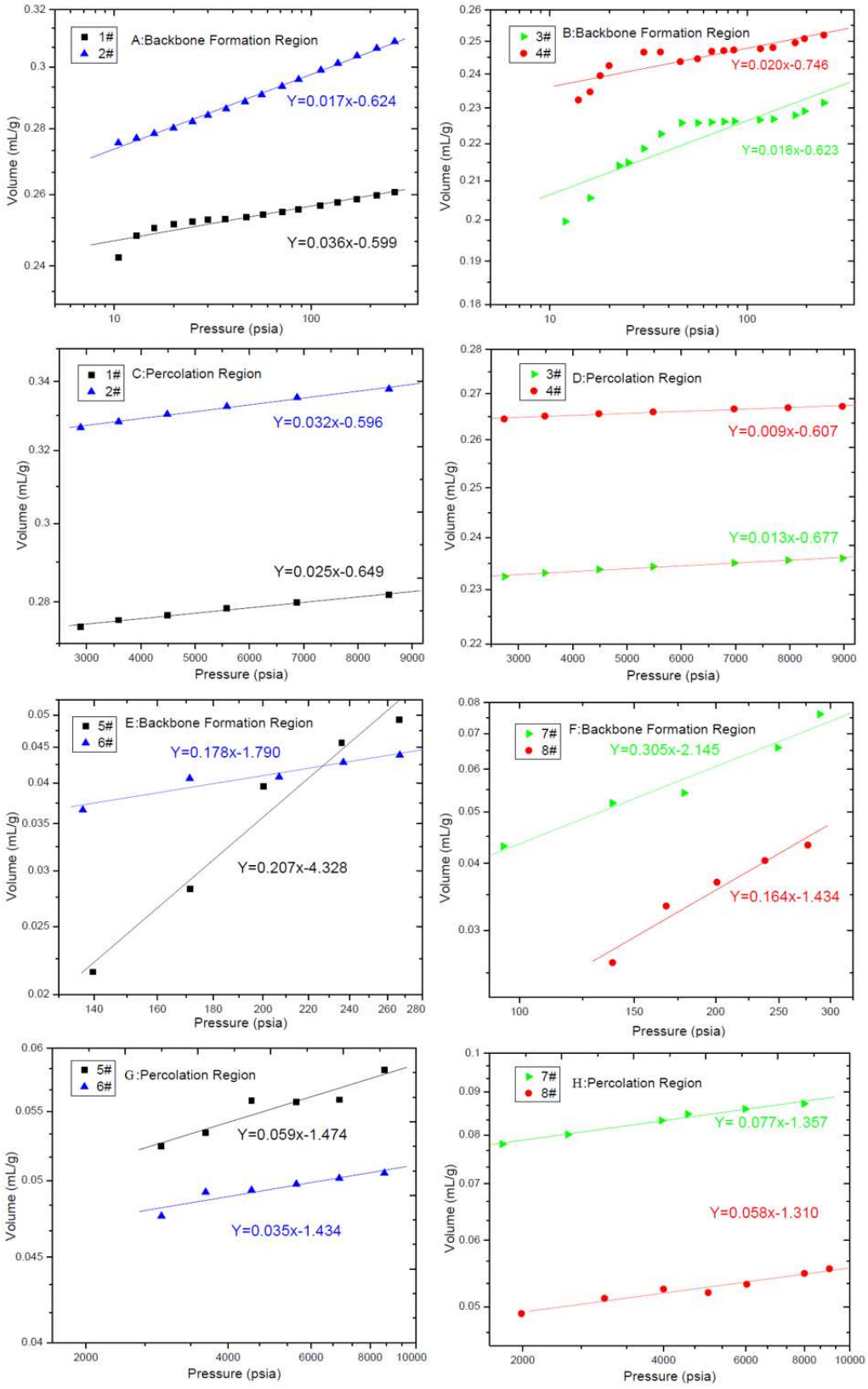

Fig.1 The double logarithmic relationship of V-ΔP in different regions for porous graphite samples

As shown in Table 2, the FDs of the samples1-4# in the percolation region are between 2.968 and 2.991 with the correlation coefficients between 0.997 and 0.999, and the root mean square (RMS)

errors between 0.0001 and 0.0003 mL/g. Correspondingly, the FDs in the backbone formation region are between 2.964 and 2.984, with the correlation coefficients between 0.906 and 0.998, and the RMS errors between 0.0006 and 0.0065 mL/g. In contrast, the FDs of the samples 5-8# in the percolation region are between 2.923 and 2.965, with the correlation coefficients between 0.990 and 0.996, and the RMS errors between 0.0001 and 0.0052 mL/g. Correspondingly, the FDs in the backbone formation region are between 2.695 and 2.836, with the correlation coefficients between 0.945 and 0.962, and the RMS errors between 0.0010 and 0.0047 mL/g. The comparison suggests that the FDs of the percolation region (2.923-2.991) are higher than those of the backbone formation region (2.695-2.984). Meanwhile the percolation region demonstrates better linearity and fewer RMS errors in corresponding curves than the backbone region. Generally, the results included in Table 2 show an excellent linear correlation, with R^2 from 0.906 to 0.999.

Table 2 Results of FDs of porous graphite samples

Sample No.	Region	Relation Equation	$\frac{\log(V)}{\log(\Delta P)}$	D	R^2	RMS Error mL/g
1#	Backbone	Y=0.017x-0.624	0.017	2.983	0.955	0.0014
	Percolation	Y=0.025x-0.649	0.025	2.975	0.999	0.0002
2#	Backbone	Y=0.036x-0.599	0.036	2.964	0.998	0.0006
	Percolation	Y=0.032x-0.596	0.032	2.968	0.997	0.0003
3#	Backbone	Y=0.020x-0.746	0.020	2.980	0.906	0.0065
	Percolation	Y=0.013x-0.677	0.013	2.987	0.998	0.0001
4#	Backbone	Y=0.016x-0.623	0.016	2.984	0.909	0.0043
	Percolation	Y=0.009x-0.607	0.009	2.991	0.999	0.0001
5#	Backbone	Y=0.207x--4.328	0.207	2.793	0.945	0.0047
	Percolation	Y=0.059x-1.474	0.059	2.941	0.996	0.0001
6#	Backbone	Y=0.178x-1.790	0.178	2.822	0.962	0.0010
	Percolation	Y=0.035x-1.434	0.035	2.965	0.995	0.0001
7#	Backbone	Y=0.305x-2.145	0.305	2.695	0.953	0.0034
	Percolation	Y= 0.077x-1.357	0.077	2.923	0.992	0.0016
8#	Backbone	Y=0.164x-1.434	0.164	2.836	0.955	0.0033
	Percolation	Y=0.058x-1.310	0.058	2.942	0.990	0.0052

For the same region, the FDs of the filtration porous graphite are higher than those of the porous graphite for impregnation. For example, in the percolation regions, the FDs of samples 1-4# are between 2.968 and 2.991, higher than the FDs of samples 5-8#, which range from 2.923 to 2.965. In the backbone region, the FDs (2.964-2.984) of samples1-4# are also higher than those of samples 5-8#, which vary from 2.695 to 2. 836.Such differences are caused by the larger number of pores and larger pore volume in the filtration graphite samples. The pores in filtration samples contribute more to the irregularity and heterogeneity of the geometry than those in the impregnation samples. However,

Table 1 and Table 2indicate that no single direct correlation is observed between the FD and the media porosity. The FD characterizes the heterogeneity and complexity of the internal structure of the fractal media without a direct relation to the porosity of the media. In other words, the FD solely characterizes the proportion of pores in the porous media. Often the higher FDs indicate a greater heterogeneity of pore structure in porous media [30,31]. Among four porous graphite samples from 1# to 4# for filtration, sample 4# demonstrates the highest FD in percolation region with a medium porosity. Sample 2# has the lowest FD in the backbone formation region with a highest porosity. Such phenomenon explains the easy mistakes by simply predicting the level of FD based on the porosity of porous media.

Many researchers have shown that different expressions of FDs highly depend on different pore structural parameters of fractal media, such as porosity, minimum pore size, maximum pore size, and even the throat size of the pores [32,33,44]. The pore size parameters obtaining is often affected by the accuracy of the measuring equipment and the measurement method, especially for the measurement in the nanometer scale. The MIP has shown some advantages to obtain the FDs and structural parameters. The intrusion volume (V) and pressure difference (ΔP) can be obtained with less complexity and higher accuracy than most of other methods. Moreover, the aforementioned structural parameters needed and errors caused by the measurement methods and instrument can be minimized.

3.2.3 FD of tortuosity by MIP test

The FD of the tortuosity (D_t) characterizes the degree of tortuosity of the capillary. Tyler, Wheatcraft and Yu et al. developed some expressions to describe the relationship among the FD of tortuosity (D_t),the tortuosity (τ), the capillary diameter (λ), and the representative length (L_0) of the capillary in a fractal media [35,36, 37,38].

$$D_t = 1 + \frac{\ln \tau}{\ln(L_0 / \lambda)} \qquad (6)$$

Eq. (6) is an ideal expression for a single capillary path. However, most of porous medium contains a large number of capillary paths. Therefore, the average tortuosity (τ_{av}) and the average pore diameter (λ_{av}) are usually preferred to τ and λ , respectively. Consequently, Eq. (6) is shown is modified as follows.

$$D_t = 1 + \frac{\ln \tau_{av}}{\ln(L_0 / \lambda_{av})} \qquad (7)$$

In Yu's research, L_0 refers to the appearance length of the sample, λ_{av} is obtained from Eq. (8). The

result of D_t=1.10 is close to the value obtained by the Monte Carlo method (1.08), which indicates such a method is effective to obtain the FD of tortuosity [38].

$$\lambda_{av} = \frac{D_f}{D_f - 1} \lambda_{\min} \left[\left(\frac{\lambda_{\max}}{\lambda_{\min}} \right)^{D_f - 1} \right] \quad (8)$$

Where $\lambda_{\min}$ and $\lambda_{\max}$ are the minimum and maximum diameter of the capillary, and D_f is the FD of the capillary, which can be obtained through the box-counting method.

However, errors can occur frequently and easily during the applications. Firstly, some potential errors are identified to obtain λ_{av} by Eq. (8). On the one hand, as mentioned above, the value of $\lambda_{\max} / \lambda_{\min}$ is directly related to the measurement range and measurement accuracy of the instrument. Sometimes the real $\lambda_{\min}$ of the capillary may be much smaller than the lower limit of the instrument. On the other hand, when D_f is calculated through the box-counting method from 2-D image, the selected images from various areas from the same sample can lead to different results. In addition, with a few exceptions such as when the sample is small enough to be captured with one image, most of images can only cover local areas, which can hardly represent the whole structure. Secondly, only when the capillary channel runs completely through the length direction of the sample, the length of the sample can be used as the representative length of the capillary (L_0), In most cases, the capillary in the porous medium does not extend throughout the whole length of the sample. Replacing L_0 with the sample length is hardly accurate.

In contrast, λ_{av} and τ_{av} can be directly obtained through the MIP test, and the potential errors associated with the Eq. (11) can be minimized. Moreover, the characteristic length of the capillary (L_c) can be obtained through the MIP tests, without considering the distribution of the capillary or whether the capillary channel runs through the whole media. Therefore, the characteristic length of the capillary (L_c) is more accurate as the representative length of the capillary (L_0) than the sample length. Eq. (7) can be modified and shown follows.

$$D_t = 1 + \frac{\ln \tau_{av}}{\ln(L_c / \lambda_{av})} \quad (9)$$

In the MIP test, the obtained λ_{av} , τ_{av} and L_c are featured with a high reliability. Therefore, calculating the FD of tortuosity of the capillary structure in porous media by following Eq. (9) offers more

advantages. Table 3 shows D_t s for eight samples. For the samples 1-4#, the tortuosity of the capillary is between 3.532 and 4.301, with the characteristic length between 15084.3 and 62998.6 nm, the average pore diameter between 227.1 and 399.8 nm, and the FDs of the tortuosity between 1.224 and 1.395. In comparison, the samples 5-8# have the tortuosity of 8.388-11.921, with the characteristic length of 5061.11-11418.2 nm, the average capillary diameter of 66.2-100.8 nm, and the FDs of the tortuosity of 1.450-1.544. The porous graphite samples for impregnation demonstrates a higher tortuosity, lower characteristic length, lower average pore diameter and higher FD of tortuosity, indicating more tortuous and complex capillary channels. In addition, no simple proportional relationship is observed between D_t with τ_{av} which makes the prediction of D_t based on the trend of τ_{av} less accurate. For example, despite that sample 3# has a higher τ_{av} than sample 4#, the D_t of sample 3# is lower than that of sample 4#,due to the lower L_c / λ_{av} ratio.

Table 3 Results of the FDs of tortuosity for porous graphite samples

Sample No.	Tortuosity τ_{av}	Characteristic length L_c (nm)	Average capillary diameter λ_{av} (nm)	FD D_t
1#	4.081	21301.5	281.7	1.325
2#	3.532	62998.6	227.1	1.224
3#	4.301	15137.3	318.6	1.378
4#	4.190	15084.3	399.8	1.395
5#	9.929	5056.1	74.6	1.544
6#	8.388	11418.2	100.8	1.450
7#	10.113	8488.2	80.5	1.497
8#	11.921	7440.1	66.2	1.525

3.3 Percolation evolution and characteristics in MIP test

Percolation theory was first proposed by Broadbent and Hammersley and has become a powerful tool for studying disorder and random phenomena in nature, and is widely used in the fields of physics, chemistry, biology, environment, finance, social problems and so on [39, 40].During the MIP test of porous graphite, an increasing amount of mercury enters the pores under the pressure gradient, and overcomes the capillary resistance to slowly intrude into the interior of the porous graphite. When the pressure reaches a certain critical point, also known as the thresholds, the intruded mercury begins to expand and fill the whole capillary network. At this point despite that the pressure continues to rise, the cumulative mercury intrusion volume no longer increases significantly. The mercury in the porous graphite has achieved a percolation distribution.

Fig.2 shows the relationship between cumulative intrusion volume and pressure for samples 1-4# during the MIP test. At the beginning of the test, only traces of (<0.03 mL/g) mercury intruded into the porous graphite, which was almost negligible. When the pressure was increased to reach the threshold value, the volume of the intruded mercury rises rapidly, and the mercury began to occupy the vacant space of the percolation region in the porous medium. According to the test, the pressures thresholds of the samples 1-4# were 8.49, 4.67, 13.05 and 11.19 psia, respectively. When the pressure rose above the threshold, the increasing of the cumulative mercury immersion volume in each sample started to slow down which corresponded to the relatively flat region in the curve, indicating that the mercury had completely intruded into the percolation network structure. When the pressure continued to increase, some new mercury continuously entered into the pores. Meanwhile an equivalent volume of mercury was pushed out of the capillary network, suggesting that the total volume within the capillary remained unchanged.

Even when the pressure was increased to 30,000 psia, the cumulative intrusion volume of mercury changed little. The process of pressurized mercury intrusion in porous graphite can be described as a process in which the fluid gradually occupies the pores, with the percolation evolution through local aggregation/gradual expansion/infinite cluster connection/global connection. In the extrusion cycle, the mercury volume demonstrated little changes, and the curve stayed flat, indicating that the anti-intrusion force was limited with a stable percolation network structure.

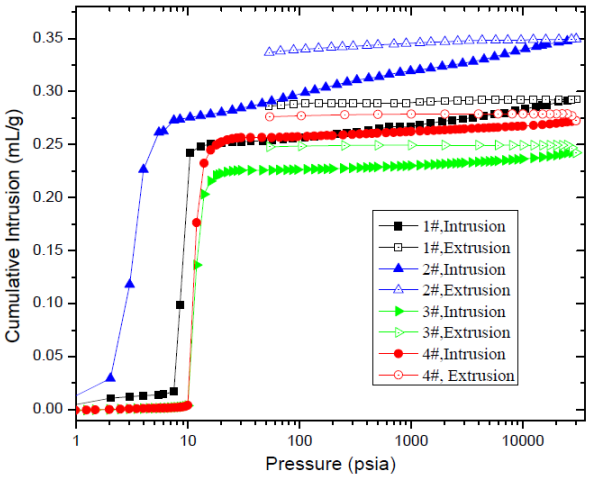

Fig.2 Relationship between cumulative intrusion volume and pressure of samples 1-4#

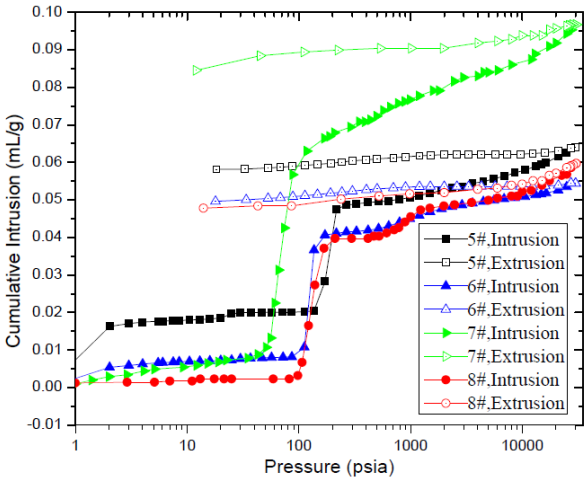

Fig.3 Relationship between cumulative intrusion volume and pressure of samples 5-8#

Fig.3 illustrates the relationship between cumulative intrusion volume and pressure for samples 5-8# during the MIP test. Comparing with the samples for filtration, the mercury intrusion volume of the samples for impregnation (0.05-0.10 mL/g) is much smaller due to the pore structure. Samples 5-8# demonstrated a lower porosity, lower average pore diameter and higher tortuosity, indicating that samples 5-8# have some more tortuous and complex capillary paths with higher flow resistance. In

other words, the mercury encountered more difficulties during the intrusion into the pores of the samples for impregnation, which is also demonstrated by the pressure thresholds. The thresholds of the samples 5-8# were 171.26, 127.53, 88.03, and 126.31 psia, much higher than those of samples 1-4#. However, two groups of samples showed similar trends in test. For example, the mercury intrusion volume increased slightly after the threshold is reached, and the total intrusion volume remained almost unchanged during the extrusion cycle. The only exception lies in Sample 7#. A considerate amount of mercury continued to intrude into the interior of the sample 7 after the threshold values was reached, showing an upward trend in the curve. When the pressure reaches 20,000 pisa, the mercury intrusion started to slow down and the increment intrusion ranged from 0.090 to 0.096 mL/g. The cumulative intrusion volume of samples 5-8# showed a flat trend in extrusion cycle, indicating that the mercury already occupies almost all interconnected pores in porous graphite.

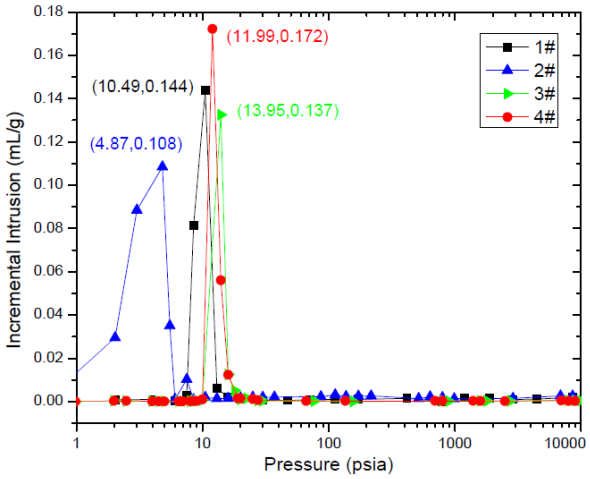

Fig.4 Relationship between incremental intrusion volume and pressure of samples 1-4#

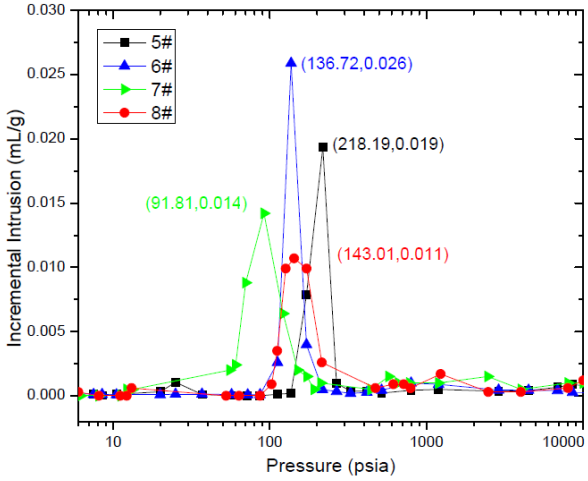

Fig.5 Relationship between incremental intrusion volume and pressure of samples 5-8#

In order to further analyze the percolation evolution of the mercury in MIP test, the relationship between the incremental intrusion volume and the pressure, and the relationship between the incremental intrusion volume and the pore size for the eight samples are shown in Figs.4 to 7. According to Fig.4, the incremental intrusion volume increased sharply when the capillary pressure got close to the threshold value. When the pressure rose slightly higher than the threshold, the incremental intrusion volumes of samples 1-4# reached the peak, which were 0.144, 0.108, 0.137, 0.172mL/g, respectively. The incremental intrusion volume rapidly dropped to near zero after the peak. In addition, no direct relation was observed between the incremental intrusion volume and the sample porosity. For example, sample 4# had the largest incremental intrusion with porosity lower than sample 1# and sample 2#.Similarly, in Fig.5, sample 6# had the highest incremental intrusion (0.026mL/g)at the threshold, with the lowest porosity (9.53%).In spite that Sample 7# had a highest porosity (15.75%),the incremental intrusion of sample 7# (0.014mL/g)at the threshold point only the ranked

number three among all samples, just a little higher than that of sample 8# (0.011mL/g).

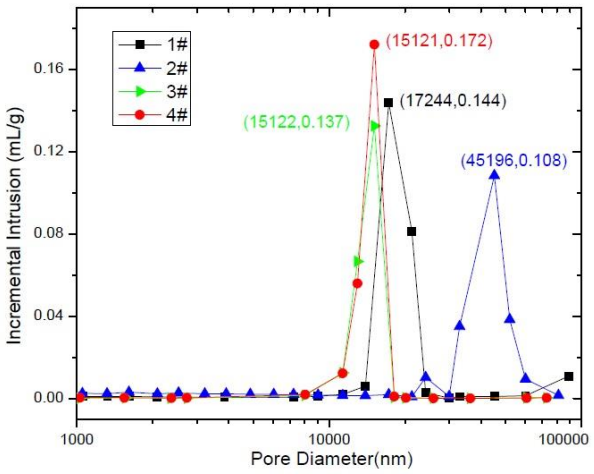

Fig.6 Relationship between incremental intrusion volume and pore size of samples 1-4#

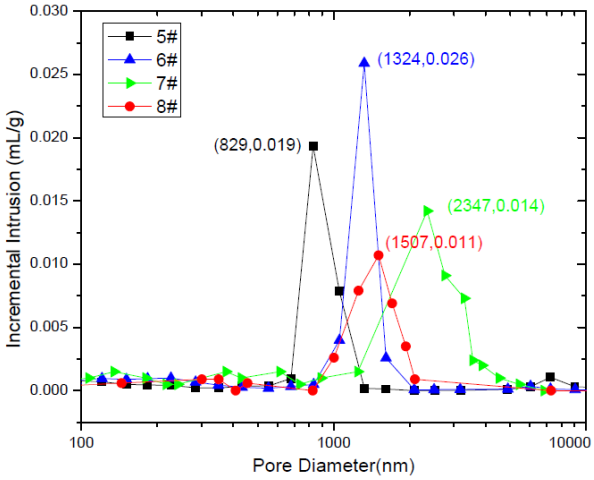

Fig.7 Relationship between incremental intrusion volume and pore size of samples 5-8#

Figs. 6-7 illustrates the relationship between the incremental intrusion and the pore size, showing various amounts of incremental intrusion at different capillary pore sizes. Fig.6 shows that the corresponding pore sizes of samples1-4# at the largest incremental intrusion volumes were 17244, 45196, 15122, and 15121 nm, and the incremental intrusion near these sizes demonstrated extremely sharp increase or decrease in trends. When the pore diameters were below these values, the mercury had not formed a percolation distribution in the pores. A more conspicuous increase was observed when the pore diameter approached closer to those values. When the pore diameters were above these values, the existing mercury achieved a percolation distribution in the pores. At this point, the mercury volume intruding into the pores is equivalent to the mercury volume flowing out of the pores. When the pore size deviated away from these values, the incremental intrusion approached closer to zero. The same trends are also shown in Fig.7. The corresponding pore sizes of the samples 5-8# at the largest incremental intrusion were 829, 1324, 2347 and 1507 nm. The incremental intrusion shows a sharp change when the pore sizes were close to these values. Consequently, Figs. 4-7 demonstrate the percolation characteristics of the microstructure and the mercury distribution in the pores. The parameters when the percolation distribution of the mercury occurred in porous media are shown in Table 4.

Table 4 Parameters of porous graphite samples at the percolation distribution of the mercury

Sample No.	1#	2#	3#	4#	5#	6#	7#	8#
Pressure (psia)	10.49	4.87	13.95	11.99	218.19	136.72	91.81	140.01
Pore diameter (*nm*)	17244	45196	15122	15121	829	1324	2347	1507
Incremental intrusion (mL/g)	0.144	0.108	0.137	0.172	0.019	0.026	0.014	0.011
Cumulative intrusion (mL/g)	0.242	0.226	0.203	0.232	0.048	0.037	0.056	0.027

4 Conclusions

The pore structural parameters of porous graphite were effectively measured and described through the MIP test. Samples for filtration have a higher porosity and average pore diameter than the samples for impregnation with a much lower tortuosity. The expression of FD for 3-D fractal media is proven to be valid to minimize the errors caused by the accuracy of measuring methods and instruments. In addition, the expression is more concise with more reliable data obtained from MIP. For all the samples, comparing with the percolation regions, the FDs in backbone formation regions are lower. The parameters of average tortuosity, characteristic length of capillary and average diameter of pores can be effectively adopted to develop the FD expression of the tortuosity of porous graphite. The parameters obtained only from MIP test offer some advantages including simplified relevant parameters with clear physical meanings, accessible measuring methods and the retrieval of reliable data, which all together contribute to the minimization of errors caused by the measurement methods and the instrument accuracy.

The microstructure of porous graphite and the intrusion evolution of mercury in pores indicate some conspicuous percolation characteristics in MIP test. The cumulative intrusion volume increases sharply as the pressure reaches the pressure threshold. After the percolation distribution of the mercury liquid in the pores, the cumulative intrusion volume demonstrates little changes even when the pressure is increased to the maximum limit. When the percolation distribution of the mercury is formed, the samples for impregnation demonstrate a much higher threshold pressure than the samples for filtration.

References

[1] Quintarda, M., Chenua, D., & Whitakerb, S. Nonlinear, multicomponent, mass transport in porous media. *Chem. Eng. Sci*.; **61**,2643-2669(2006).

[2] Ochoa-Tapia, J. A., & Whitaker, S. Heat transfer at the boundary between a porous medium and a homogeneous fluid. *Int. J. Heat. Mass. Tran*. **40**,2691-707(1997).

[3] Adler, P.M., & Thover, J. F. Fractal porous media. *Transport porous med*. **13**,41-78(1993).

[4] Mandelbrot, B. B. The fractal geometry of nature. *San Francisco: Freeman* (1982).

[5] Katz, A. J., & Thomoson, A. H. Fractal sand stone porous: Implication for conductivity and formation. *Phys. Rev. Lett.* **54**,1325-1328(1985).

[6] Winslow, D. N. Fractal character in cement and concrete. *Cement Concrete Res.* **15**,817-824(1985).

[7] Rieu, M., & Sposito, G. Fractal Fragmentation: Soil porosity and soil water properties of theory. *Soil Sci. Soc. Amer. J.* **55**,1231-1238(1991).

[8] Sun, W. J., Feng, Y. Y., Jiang, C. F., & Chu, W. Fractal characterization and methane adsorption features of coal particles taken from shallow and deep coalmine layers. *Fuel*. **155**,7-13(2015).

[9] Krohn, C. E. Fractal measurements of sandstone, hales and carbonates. *Geo. Res*. **93**, 3297-3305(1988).

[10] Tyler, S. W., & Wheatcraft, S. W. Fractal process in soil water retention. *Water Resour. Res*. **26**,1047-1054(1990).

[11] Nie, B. S. *et al*. Pore structure characterization of different rank coals using gas adsorption and scanning electron microscopy. *Fuel*. **158**,908-107(2015).

[12] Carriazo, J. G., Molina, R., & Moreno, S. Fractal dimension and energetic heterogeneity of gold-modified Al–Fe–Ce. *Appl. Surf. Sci*. **255**, 3354-3360(2008).

[13] Zhang, J. R., Huang, L., Zhu, J., & Huang, W. J. SEM Analysis of Soil Pore and its Fractal Dimension on Micro-scale. *Acta Pedologica Sinica*. **45**,207-215(2008).

[14] Go´mez-Carracedo, A. *et al*. Fractal analysis of SEM images and mercury intrusion porosimetry data for the microstructural characterization of microcrystalline cellulose-based pellets. *Acta Mater*. **57**,295-303(2009).

[15] Yao, Y. B. *et al*. Fractal characterization of seepage-pores of coals from China: An investigation on permeability of coals. *Comput. Geosci*. **6**, 1159-1166(2009).

[16] Wu, Y. Q. *et al*. A comprehensive study on geometric, topological and fractal characterizations of pore systems in low-permeability reservoirs based on SEM, MICP, NMR, and X-ray CT experiments. *Mar. Petrol. Geo.***103**,12-28(2019).

[17] Wang, Q. L. Study on Formation and Percolation Mechanism of Pores and Permeability in Graphite Porous Media. *China Unive. Min. Technol. Press, Xuzhou*, China (2011).

[18] Wang, Q. L., He, M., He, Y. Q., & Han, J. Fractal characteristics of the microstructure for porous graphite. *Mate. Res. Innov.* **19(S1)**,459-464(2015).

[19] Yelena, V., & Thomas, J. M. Multifractal-based assessment of Gilso carbon graphite Microstructures. *Carbon.* **109**,711-718(2016).

[20] Liu, Q. S. *et al*. Pore and fractal characteristics of graphite lining based on micro CT. *Mater. Sci. Technol.* **26**,59-65. (2018, In Chinese)

[21] Washburn, E. W. The dynamics of capillary flow. *Phys. Rev.* **17**, 273-283(1921).

[22] Kate, J. M., Gokhale, C. S. A simple method to estimate complete pore size distribution of rocks. *Eng. Geol.* **84**,48-69(2006).

[23] Tsakiroglou, C., & Payatakes, A. Mercury Intrusion and Retraction in Model Porous Media, *Adv. Colloid. Interface Sci.***75**,215-253(1998).

[24] Rashid, F. *et al*. Permeability prediction in tight carbonate rocks using capillary pressure measurements. *Mar. Petro. Geol.* **68**,536-550(2015).

[25] Pirard, R., Alie, C., & Pirard, J. P. Characterization of porous texture of hyperporous materials by mercury porosimetry using densification equation. *Powder. Technol.* **128**,242- 247(2002).

[26] Carlos A. L. Y. L. New perspectives in mercury porosimetry. *Adv. Colloid Interface Sci.* **76-77**,341-372(1998).

[27] Dubuc, B. *et al*. Evaluating the Fractal Dimension of Surfaces, *Proceedings of the Royal Society of London. Series A*. **425**,113-127(1989).

[28] Yu, B. M. Advance of fractal analysis of transport properties for porous media. *Adv. mech.* **33**,333-346(2003).

[29] Alvarodo, R. F., Alvarodo. V., & Gonzalez, H. Fractal dimensions form mercury intrusion capillary tests, *Society of Petroleum Engineers.* Caracas, Venezuela.255-233(1992).

[30] Li, K., & Horne, R. N. Fractal modeling of capillary pressure curves for the Geysers rocks. *Geothermics*. **35**,198-207(2006).

[31] Jin, L., & Wang, G. Fractal analysis of tight gas sandstones using high-pressure mercury intrusion techniques. *J. Nat. Gas Sci. Eng.* **24**,185-196(2015).

[32] Hunt, A. G., & Skinner, T. E. Incorporation of Effects of Diffusion into Advection-Mediated Dispersion in Porous Media. *J. Stat. Phys.* **140**, 544-564(2010).

[33] Rieu, M., & Sposito, G. Fractal fragmentation, soil porosity, and soil water properties (I. Theory*). Soil Sci. Soc. Amer. J.* **55**,1231-1238(1991).

[34] Wei, J.X., Yu, Q.J., Zhen, X. X., & Bai, R. Y. Fractal Dimension of Pore Structure of Concrete. *J. South China Univ. Tech.*; **35**,121-124. (2007, In Chinese)

[35] Wheatcraft, S.W. & Tyler, S. W. An explanation of scale dependent dispersivity in heterogeneous aquifers using concepts of fractal geometry, *Water Resour. Res*. **24**,566-578(1988).

[36] Tyler, S. W. & Wheatcraft, S. W. Fractal scaling of soil particle-size distributions: analysis and limitations, *Soi Sci Soc Am J.* **56**,326-369(1992).

[37] Yu, B.M.& Li, J.H. Some fractal characters of porous media. *Fractal*. **9**,365-372(2001).

[38] Yu, B.M. & Cheng, P. A fractal model for permeability of bi-dispersed porous media. *Int J Heat Mass Tran.* **45**, 2983-2993(2002).

[39] Broadbent, S. R. Hammersley JM. Percolation Processes b I. Crystals and Mazes. *Proc. Camb. Phil. Soc.***53**,620-641(1957).

[40] Geoffrey, G. Percolation and disordered systems. *Lectures on Probability Theory and Statistics.* **11**,153-300(2006).

Acknowledgments

The authors acknowledge the support by the Fundamental Research Funds for the Central Universities (No. 2019GF02).

Author contribution statement

Wang Qili and Sun Jiarui wrote the main manuscript text. Chen Yuehu and Qian Yuyan carried out the experimental research. Sun Jiarui and Yan Sheng developed many further discussions on the simulation results. Fei Shengcheng prepared all the figures in manuscript and Wang Qili revised the manuscript text.

Competing Interests statement

The authors declare no competing interests.